The Astrophysical Journal, 923:234 (6pp), 2021 December 20 https://doi.org/10.3847/1538-4357/ac300d

Near-infrared and Visible Opacities of S-type Stars: The $B^1\Pi$—$X^1\Sigma^+$ Band System of ZrO

Jason J. Sorensen and Peter F. Bernath
Department of Chemistry and Biochemistry, Old Dominion University, Norfolk, VA 23529, USA; jsorense@odu.edu
Received 2021 September 8; revised 2021 October 5; accepted 2021 October 11; published 2021 December 24

Abstract

The ZrO $B^1\Pi$—$X^1\Sigma^+$ transition is an important opacity source in the near-infrared and optical spectrum of S-type stars. The 0–0, 0–1, 0–2, 1–0, 1–2, 1–3, 2–0, 2–1, 2–3, 2–4, 3–1, 3–4, and 4–2 bands of the $^{90}Zr^{16}O$ $B^1\Pi$—$X^1\Sigma^+$ transition are reanalyzed using a high-temperature (2390 K) high-resolution (0.04 cm^{-1}) emission spectrum collected at the National Solar Observatory (Kitt Peak). A modern spectroscopic analysis was performed using the PGOPHER program to provide updated spectroscopic constants and to produce a high-precision line list with line strengths based on an ab initio calculation of the transition dipole moment.

Unified Astronomy Thesaurus concepts: High resolution spectroscopy (2096); S stars (1421); Zirconium stars (1844); Spectral line lists (2082)

Supporting material: FITS files, tar.gz file

1. Introduction

Like many transition metal diatomic molecules, ZrO has a very complicated electronic band structure and possesses many strong absorption features. These absorption bands are the defining characteristic of S-type stars (Keenan 1954) as first reported by Merrill (1922) and later confirmed to originate from molecular ZrO by King (1924). It was claimed by Piccirillo (1980) and later confirmed by Van Eck et al. (2017) that these strong ZrO bands stem from an abnormally large concentration of slow neutron-capture process (s-process) elements of which Zr is one. ZrO bands have also been observed in SC-type stars (Keenan & Boeshaar 1980; Zijlstra et al. 2004), M-stars (Bobrovnikoff 1934), and sunspots (Richardson 1931; Sriramachandran & Shanmugavel 2012).

As ZrO is of considerable astrophysical importance, it has been experimentally analyzed on many occasions, with McKemmish et al. (2018) providing an excellent review of these studies. Many of these studies are beyond the scope of this work, and our literature review focuses on only those studies that are most pertinent to our analysis of the $B^1\Pi$—$X^1\Sigma^+$ band system. The 0–0 band of the $B^1\Pi$—$X^1\Sigma^+$ transition was first observed at high resolution by Balfour & Tatum (1973) by recording the emission spectra of ZrO on photographic plates using a zirconium arc source. Phillips & Davis (1976) were able to observe 18 bands with ground-state vibrational levels ranging up to $v''=7$ and excited-state levels up to $v'=5$, using emission data obtained from a carbon furnace and a spectrograph.

Microwave studies for ZrO were first performed by Suenram et al. (1990) where they were able to measure the $X^1\Sigma^+$ $J=1$–0 transition frequency for the $v=0$ band using a Fourier-transform microwave spectrometer coupled with a laser ablation molecular source. Using cavity microwave spectroscopy, Beaton & Gerry (1999) were able to expand on Suenram et al.'s work to measure the $X^1\Sigma^+$ $J=1$–0 transition frequencies for $v=0$, 1, 2, and 3. Other experimental studies include line-intensity absorption studies by Littleton et al. (1993) and Littleton & Davis (1985) using a high-temperature furnace source and a Fourier-transform spectrometer (FTS) to determine the transition dipole moment. Pettersson et al. (2000) determined the permanent electric dipole moment of the $B^1\Pi$ state by observing the first-order Stark effect in a molecular beam.

ZrO has been the subject of many theoretical studies with only a few noted here. First, Langhoff & Bauschlicher (1990) report spectroscopic constants of ZrO that were calculated using a modified coupled-pair functional method (MCPF) (Langhoff & Bauschlicher 1988). Second, Langhoff & Bauschlicher (1990) did a follow up study reporting electronic transition moment functions and radiative lifetimes for ZrO using the state-averaged, complete active space self-consistent field (SA-CASSCF) method which was followed up by a multi-reference configuration-interaction (MRCI) treatment to handle electron correlation (Langhoff & Bauschlicher 1990). More recently, spectroscopic constants for the lowest 13 singlet and triplet states were calculated by Tabet et al. (2019) using CASSCF and MRCI-SD (multi-reference configuration-interaction with single and double excitation) methods.

Although the $B^1\Pi$—$X^1\Sigma^+$ transition has been studied in the past, as indicated above, most of the spectral line assignments have escaped modern analysis made possible by high resolution spectroscopic methods like Fourier transform spectroscopy, and modern spectroscopic fitting programs such as PGOPHER. Furthermore, a spectral line list that includes line intensities has never been published; however, an unpublished line list, put together by Plez et al. (2003), is available upon request. These line lists are essential tools needed to simulate spectral energy distributions of astronomical sources. In this work we report updated spectroscopic constants by fitting 13 bands of the $B^1\Pi$—$X^1\Sigma^+$ transition using a high-resolution spectrum of the emission of high temperature ZrO as detected using an FTS.

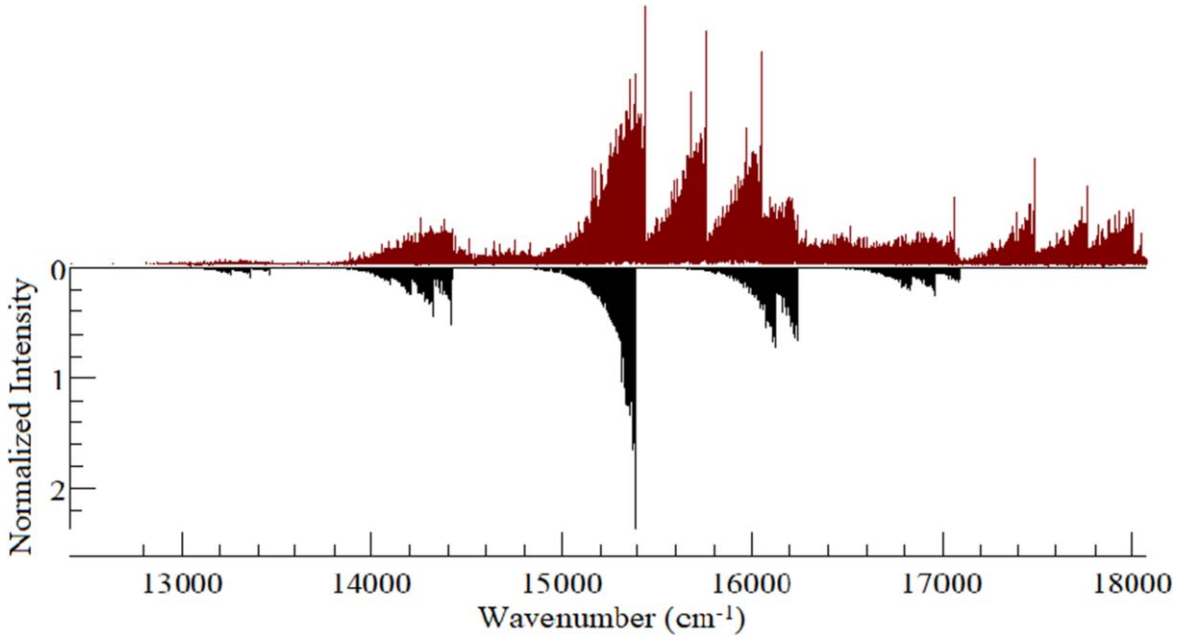

Figure 1. An overview of the $^{90}Zr^{16}O$ spectrum (red, upward) along with the simulation (black, downward) for 13 bands of the ZrO, $B^1\Pi$—$X^1\Sigma^+$ transition. Note that spectral features not simulated largely originate from bands associated with the ZrO, $d^3\Phi$ - $a^3\Delta$ transition, which are not studied in this work.

2. Method and Results

The spectra of ZrO used in this analysis were collected by S. Davis at the National Solar Observatory (Kitt Peak). ZrO was produced using a carbon tube furnace that contained a few grams of ZrO_2, charged with 110 Torr helium, and heated to 2390 K. Over about an hour of integration time, eight emission scans were added using UV-enhanced Si photodiode detectors and a 1 m Fourier-transform spectrometer at high resolution ($0.04\,cm^{-1}$). The frequency axis was calibrated using Simard et al.'s (1988) ZrO $C^1\Sigma^+$-$X^1\Sigma^+$ 0–0 band lines obtained from laser-induced fluorescence of a supersonically cooled ZrO molecular beam. This calibration was then compared to Pettersson et al.'s (2000) ZrO $B^1\Pi$—$X^1\Sigma^+$ 0–0 line positions obtained via resonant two-photon ionization (R2PI) time-of-flight mass spectroscopy. The Simard calibration of the spectrum was found to agree with Pettersson et al.'s line positions to within about $0.005\,cm^{-1}$. We therefore estimate the absolute error in our line position measurements for unblended strong lines to be $0.005\,cm^{-1}$.

Spectral fitting was performed with the PGOPHER program (Western 2017) using Phillips & Davis's (1976) constants as initial ZrO $B^1\Pi$—$X^1\Sigma^+$ parameters. Ground-state microwave data for $v = 0$, 1, 2, and 3 of the $X^1\Sigma^+$ $J = 1$–0 transition from Suenram et al. (1990) and Beaton & Gerry (1999) were also used in the PGOPHER fit. Standard energy level expressions were used as they can be output from PGOPHER. In all cases each line fitted retained PGOPHER's default standard deviation weighting of 1 except for the four microwave lines, which had their weightings switched to 0.02 ($v = 0$), 0.002 ($v = 1$), 0.2 ($v = 2$), and 0.02 ($v = 3$). An overview of the spectrum analyzed (red, upward) and the accompanying simulation (black, downward) are displayed in Figure 1. New constants were incorporated into the fit as higher J values were added. The spectrum analyzed had a high spectral line density with many overlapping and blended transitions that made definitive assignments difficult for higher vibrational levels ($v > 4$). However, we routinely were able to assign transitions with J values in excess of 100 and typically in the $J = 180$–200 range. An example of a typical region of the fit is shown in Figure 2 depicting the R branch head of the 3–4 band (blue downward trace). This image also illustrates some of the spectral blending that was observed during this analysis with lines associated with the 1–2 (purple downward trace), 2–3 (red downward trace), and 0–1 (green downward trace) bands that are also seen in this region. The spectroscopic constants that produced this fit are shown in Table 1. Ultimately, 4080 lines associated with the 0–0, 0–1, 0–2, 1–0, 1–2, 1–3, 2–0, 2–1, 2–3, 2–4, 3–1, 3–4, and 4–2 bands were fitted with an average error of $0.012\,cm^{-1}$. The full list of fitted lines is available online as a PGOPHER log file, and a sample is shown with the observed minus calculated values in Table 2.

The next objective after accomplishing this spectral fit was to produce a line list that includes spectral line strengths. This was accomplished using the RKR and LEVEL programs of Le Roy (2017a, 2017b). The RKR program provides potential energy surfaces for a diatomic molecule's ground and excited states by implementing the first-order semi-classical Rydberg–Klein–Rees (RKR) method. In the RKR method, these potential energy surfaces are determined from knowing the vibrational quantum number (v) dependence of the molecular vibrational energies, G_v, and the inertial rotational constants, B_v, as shown in Equations (1) and (2):

$$G_v = \omega_e\left(v+\frac{1}{2}\right) - \omega_e x_e\left(v+\frac{1}{2}\right)^2 + \omega_e y_e\left(v+\frac{1}{2}\right)^3 + ..., \quad (1)$$

$$B_v = B_e - \alpha_e\left(v+\frac{1}{2}\right) + \gamma_e\left(v+\frac{1}{2}\right)^2 + \delta_e\left(v+\frac{1}{2}\right)^3 + ... \quad (2)$$

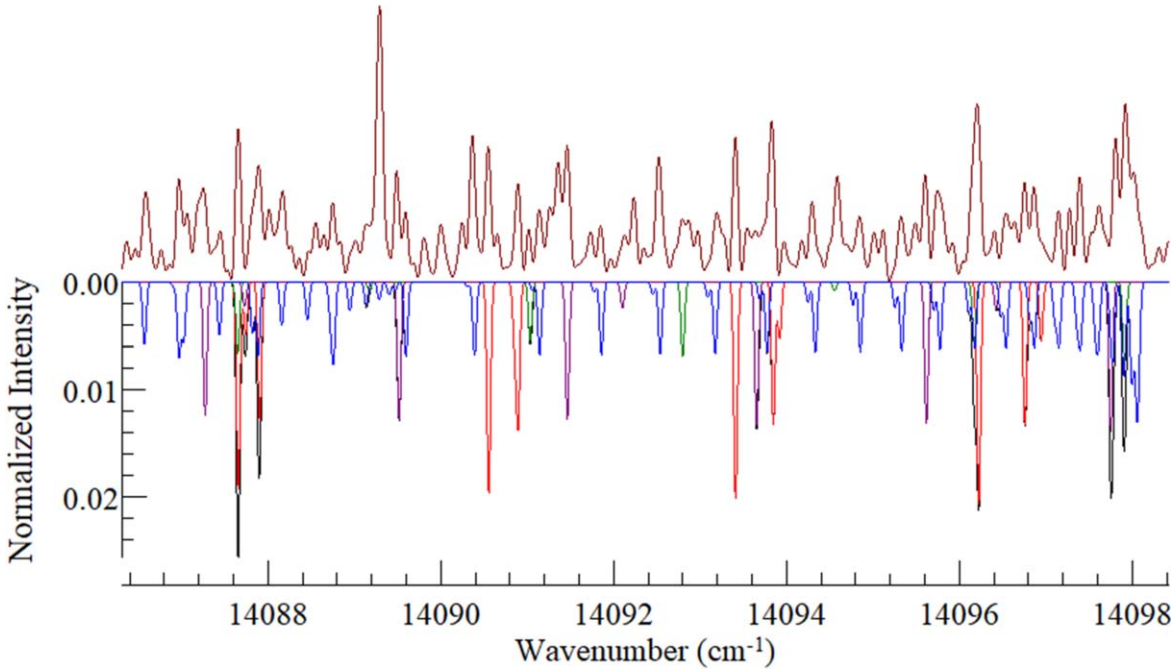

Figure 2. Typical $^{90}Zr^{16}O$, $B^1\Pi$—$X^1\Sigma^+$ spectrum (red, upward) with simulated *R* branch head for the 3–4 band (blue, downward trace). Also shown are lines associated with the $^{90}Zr^{16}O$, $B^1\Pi$—$X^1\Sigma^+$ 1–2 (purple, downward trace), 2–3 (red, downward trace), and 0–1 (green, downward trace) bands, which give an indication to the degree of spectral line blending that was observed throughout this study.

Table 1
$^{90}Zr^{16}O$ Spectroscopic Constants of the $X^1\Sigma^+$ and $B^1\Pi$ States for $v = 0$–4 in cm^{-1} with One Standard Deviation Error Indicated in Parentheses as Obtained from PGOPHER

$X^1\Sigma^+$					
v	0	1	2	3	4
T_v	0	969.5265(15)	1932.1640(15)	2887.9318(15)	3836.8025(19)
B_v	0.4226094(42)	0.4206550(42)	0.4187073(42)	0.4167260(43)	0.4147137(43)
$D_v \times 10^7$	3.1655(28)	3.1719(26)	3.2198(29)	3.1988(29)	3.0660(30)
$H_v \times 10^{13}$	−0.897(67)	−1.028(45)	2.257(71)	1.21(76)	−1.128(82)
$L_v \times 10^{18}$	0.338(76)	⋯	−5.551(78)	−1.774(83)	−2.009(98)
$B^1\Pi$					
v	0	1	2	3	4
T_v	15383.4185(12)	16236.9756(12)	17084.6239(13)	17926.3193(20)	18762.0185(26)
B_v	0.4015161(42)	0.3995955(42)	0.3976571(42)	0.3957073(43)	0.3937782(47)
$D_v \times 10^7$	3.4959(27)	3.5012(29)	3.4477(28)	3.4231(30)	3.5477(52)
$H_v \times 10^{12}$	−0.0631(58)	−0.0826(72)	−1.1882(70)	−2.1743(92)	0.0758(278)
$L_v \times 10^{16}$	0.00223(53)	0.00384(77)	0.32933(77)	1.53345(132)	⋯
$q_v \times 10^4$	−2.3917(59)	−2.3402(60)	−2.3823(65)	−2.644(11)	−2.272(12)
$q_{Dv} \times 10^8$	0.1501(94)	0.1198(101)	0.7687(115)	2.225(200)	0.0954(150)
$q_{Hv} \times 10^{12}$	−0.0131(46)	−0.0209(50)	−1.0743(60)	−4.5499(117)	⋯
$q_{Lv} \times 10^{16}$	−0.00158(68)	0.00103(75)	−0.00340(95)	3.2072(21)	⋯

The constants ω_e, $\omega_e x_e$, $\omega_e y_e$, α_e, γ_e, and δ_e are determined from the spectroscopic constants in Table 1 and are shown for the ZrO ground $X^1\Sigma^+$ and excited $B^1\Pi$ states in Table 3 along with previously reported values.

These RKR potential energy surfaces are then combined with the ZrO $B^1\Pi$—$X^1\Sigma^+$ transition dipole moment function, as calculated by Langhoff & Bauschlicher (1990), as the input for Le Roy's LEVEL program. As Langhoff & Bauschlicher (1990) only reported seven transition dipole moment points for ZrO bond lengths between 2.80 and 3.60 a_0 (1.48–1.91 Å), we fit these points to a fourth-order polynomial and extrapolated 424 in-between points using a step size of 0.001 Å. The LEVEL input file is available online. This file contains both the RKR ground- and excited-state potential energy surfaces and the extended transition dipole moment function used in this analysis.

LEVEL solves the one-dimensional Schrödinger equation to calculate a number of different parameters such as Franck–Condon factors, and band strengths as shown in Table 4. Additionally, Table 4 includes derived Einstein A band coefficients ($A = 3.136 \times 10^{-7}\ \nu^3 S$) where the band origin, ν (cm^{-1}) is taken from PGOPHER and S is the square of the

Table 2
Sample of Lines and Residuals of the 0–0, 0–1, 0–2, 1–0, 1–2, 1–3, 2–0, 2–1, 2–3, 2–4, 3–1, 3–4, and 4–2 Bands of $^{90}Zr^{16}O$ $B^1\Pi$-$X^1\Sigma^+$ Transition Taken from the PGOPHER Log File

J′	P′	J″	P″	Obs (cm^{-1})	Calc (cm^{-1})	O–C (cm^{-1})	Line Assignment	Source
1	e	2	e	15381.6947	15381.6856	0.0091	P(2) : B 1pi $v = 0$ 1 e—X 1 sigma $v = 0$ 2 e	1: ⟨ Linelist⟩
4	e	5	e	15378.7616	15378.7683	−0.0067	P(5) : B 1pi $v = 0$ 4 e—X 1 sigma $v = 0$ 5 e	2: ⟨ Linelist⟩
6	e	7	e	15376.6075	15376.6114	−0.0039	P(7) : B 1pi $v = 0$ 6 e—X 1 sigma $v = 0$ 7 e	3: ⟨ Linelist⟩
8	e	9	e	15374.2849	15374.285	−0.0001	P(9) : B 1pi $v = 0$ 8 e—X 1 sigma $v = 0$ 9 e	4: ⟨ Linelist⟩
12	e	13	e	15369.1027	15369.1234	−0.0207	P(13) : B 1pi $v = 0$ 12 e—X 1 sigma $v = 0$ 13 e	5: ⟨ Linelist⟩
13	e	14	e	15367.7248	15367.7271	−0.0023	P(14) : B 1pi $v = 0$ 13 e—X 1 sigma $v = 0$ 14 e	6: ⟨ Linelist⟩
15	e	16	e	15364.8068	15364.8072	−0.0004	P(16) : B 1pi $v = 0$ 15 e—X 1 sigma $v = 0$ 16 e	7: ⟨ Linelist⟩
16	e	17	e	15363.2799	15363.2837	−0.0038	P(17) : B 1pi $v = 0$ 16 e—X 1 sigma $v = 0$ 17 e	8: ⟨ Linelist⟩

Note. J is total angular momentum, P is the e/f parity, Obs is the observed line position in cm^{-1}, Calc is the calculated line position in cm^{-1}, and O–C is the observed minus calculated line position in cm^{-1}. (This table is available in its entirety as a .log file).
(This table is available in its entirety in FITS format.)

Table 3
Equilibrium Molecular Constants for the $^{90}Zr^{16}O$ $B^1\Pi$—$X^1\Sigma^+$ Transition along with Previously Reported Values in cm^{-1} Except the Equilibrium Bond Length, r_e, which is in Å

$X^1\Sigma^+$	This Work	Previous Values
ω_e	976.40869(593)	976.51[a]
$\omega_e x_e$	3.44153(116)	3.462[a]
$\omega_e y_e$	…	0.00052[a]
B_e	0.4235669(134)	0.423608[a]
α_e	1.9186(126)E-03	1.95E-03[a]
γ_e	−1.068(246)E-05	−3.30E-06[a]
δ_e	…	6.66E-11[a]
r_e(Å)	1.71199404(79)	1.71195242(73)[b] 1.71387(13)[c]
$B^1\Pi$		
ω_e	859.424252(344)	859.44[a]
$\omega_e x_e$	2.921697(161)	2.918[a]
$\omega_e y_e$	−7.2866(212)E-03	−0.00812[a]
B_e	0.402460322(736)	0.402501[a]
α_e	1.8770(132)E-03	1.920E-03[a]
γ_e	−2.611(618)E-05	−5.0E-06[a]
δ_e	3.211(816)E-06	…
r_e(Å)	1.75631230(44)	1.75831(13)[c]

Notes. All values are reported with one standard deviation error indicated in parentheses.
[a] Values are from Phillips & Davis (1976) and were reported without error estimates.
[b] Values are from Beaton & Gerry (1999).
[c] Values are from Pettersson et al. (2000).

Table 4
$^{90}Zr^{16}O$ Band Intensities and Franck–Condon Factors Taken from the LEVEL Program along with Calculated Einstein A Values for the Bands (See the Text)

Band	Band Strengths ($\langle v'\|\mu\|v''\rangle$) (D)	Franck–Condon Factors	Einstein A (s^{-1})
0–0	3.12849	6.9413E-01	1.1175E+07
1–0	1.97565	2.5127E-01	5.2401E+06
2–0	0.90291	4.7785E-02	1.2750E+06
3–0	0.34042	6.1813E-03	2.0936E+05
4–0	0.11041	5.8854E-04	2.5252E+04
0–1	1.78849	2.5475E-01	3.0041E+06
1–1	1.96918	2.7832E-01	4.3279E+06
2–1	2.25859	3.3244E-01	6.6954E+06
3–1	1.36564	1.1072E-01	2.8517E+06
4–1	0.62065	2.0832E-02	6.8047E+05
0–2	0.71353	4.5664E-02	3.8861E+05
1–2	2.06283	3.4359E-01	3.9064E+06
2–2	1.02318	7.5953E-02	1.1422E+06
3–2	2.18574	3.1509E-01	6.1303E+06
4–2	1.67125	1.6798E-01	4.1757E+06
0–3	0.22280	5.0662E-03	3.0374E+04
1–3	1.08924	1.0794E-01	8.8512E+05
2–3	2.02293	3.3512E-01	3.6722E+06
3–3	0.26977	5.2928E-03	7.7622E+04
4–3	1.93091	2.4871E-01	4.6773E+06
0–4	0.05636	3.7496E-04	1.5335E+03
1–4	0.40725	1.7187E-02	9.9177E+04
2–4	1.35137	1.6861E-01	1.3316E+06
3–4	1.83098	2.7875E-01	2.9407E+06
4–4	0.30611	7.0387E-03	9.7704E+04

band strength in debye^2 (Bernath 2020). The calculated band strengths were then put into PGOPHER, to determine the line strengths. PGOPHER was used to output a complete line list for all possible bands up to $J = 200$, which is included online as an edited PGOPHER .out file, with a sample displayed as Table 5.

3. Discussion

The spectroscopic constants found in Table 1 that are derived from the fit lines listed in Table 2 extend the previous analysis from a maximum J of about 100 to a maximum J of about 200 for the 0–0, 0–1, 0–2, 1–0, 1–2, 1–3, 2–0, 2–1, 2–3, 2–4, 3–1, 3–4, and 4–2 bands. Phillips & Davis (1976) reported line assignments for the 3–5, 3–6, 4–5, 4–6, 5–3, and 5–7 bands in addition to the bands studied herein. An attempt was made to extend this study to all these bands; however, this proved to be very difficult. This difficulty was due to a number of issues such as the large number of observed lines, decreasing band intensity, and the propensity of these lines to be overlapped and blended with other $B^1\Pi$—$X^1\Sigma^+$ transition lines or lines associated with the $d^3\Phi$–$a^3\Delta$ transition. Bands associated with the $d^3\Phi$–$a^3\Delta$ transition are often quite intense but are not analyzed by us at this time; however, we intend to analyze them in the near future. Even with Phillips & Davis's lines as a guide, it proved too difficult to fit these higher bands with confidence, so they were excluded.

Table 5
Sample Table of the PGOPHER Line List for the 0–0, 0–1, 0–2, 1–0, 1–2, 1–3, 2–0, 2–1, 2–3, 2–4, 3–1, 3–4, and 4–2 Bands of the $^{90}Zr^{16}O$ $B^1\Pi$-$X^1\Sigma^+$ Band System

J′	J″	Pos (cm^{-1})	Eup (cm^{-1})	Elow (cm^{-1})	A (s^{-1})	f × 10^3	Line Assignment
90	89	13381.9744	18647.4191	5265.4447	1.924E+05	1.629	R(89)B1pi $v = 0$ 90e -X 1sigma $v = 2$ 89e
42	43	13383.9952	16107.2024	2723.2072	1.892E+05	1.547	P(43)B1pi $v = 0$ 42e-X1sigma $v = 2$ 43e
62	62	13384.1243	16946.8590	3562.7346	3.828E+05	3.204	Q(62)B1pi $v = 0$ 62f-X1sigma $v = 2$ 62e
89	88	13384.3703	18576.1874	5191.8171	1.925E+05	1.629	R(88)B1pi $v = 0$ 89e-X1sigma $v = 2$ 88e
180	181	13384.8436	29651.7806	16266.9370	1.535E+06	1.277	P(181)B1pi $v = 2$ 180e-X1sigma $v = 3$ 181e
185	185	13386.1741	31122.8347	17736.6606	2.522E+06	2.110	Q(185)B1pi $v = 3$ 185f-X1sigma $v = 4$ 185e
61	61	13386.2697	16897.3904	3511.1208	3.830E+05	3.204	Q(61)B1pi $v = 0$ 61f-X1sigma $v = 2$ 61e
41	42	13386.2879	16073.5885	2687.3006	1.892E+05	1.546	P(42)B1pi $v = 0$ 41e-X1sigma $v = 2$ 42e
88	87	13386.7278	18505.7248	5118.9970	1.926E+05	1.630	R(87)B1pi $v = 0$ 88e-X1sigma $v = 2$ 87e
193	194	13388.2938	30700.2184	17311.9246	1.597E+06	1.329	P(194)B1pi $v = 1$ 193e-X1sigma $v = 2$ 194e

Note. J is the total angular momentum, Pos is the calculated line position in cm^{-1}, Eup and Elow are the upper and lower energy levels in cm^{-1}, A is the Einstein $A_{J' \rightarrow J''}$ value in s^{-1}, and $f_{J' \leftarrow J''}$ is the oscillator strength, and line assignments are the associated quantum numbers for the given transition. (This table is available in its entirety as a PGOPHER .out file).
(This table is available in its entirety in FITS format.)

Table 3 shows the derived equilibrium molecular constants associated with the ZrO $X^1\Sigma^+$ ground state and $B^1\Pi$ excited state, along with previous reported values. Previous values for ω_e, $\omega_e x_e$, $\omega_e y_e$, B_e, α_e, γ_e, and δ_e come from Phillips & Davis's (1976) work for which no error limits were reported. A third-order polynomial fit was attempted on the ground state in order to determine the $\omega_e y_e$ and γ_e constants; however, the errors in these higher-order terms turned out to be too large to report values, so only the second-order results are reported in Table 3. The equilibrium bond lengths, r_e in Å, were calculated from the equilibrium rotational constant, B_e in cm^{-1}, as found in Table 3, using the standard equations (Bernath 2020). For the calculation of the reduced mass of $^{90}Zr^{16}O$, the atomic masses were taken from the new atomic mass evaluation, AME2020 (Huang et al. 2021; Wang et al. 2021). Using the band intensities from LEVEL (Table 4) in PGOPHER, a complete line list for all bands with v', $v'' < 5$ can be exported as shown in Table 5. The Einstein $A_{J'-J''}$ values were converted to oscillator strengths $f_{J' \leftarrow J''}$ (Bernath 2020) using

$$f_{J' \leftarrow J''} = \frac{1.499194}{\tilde{\nu}^2} \frac{2J' + 1}{2J'' + 1} A_{J' \rightarrow J''}, \quad (3)$$

with $\tilde{\nu}$ in cm^{-1}. These line strengths were added to the PGOPHER .out file as a separate column.

The error in our reported line strengths is difficult to judge, however, an estimate can be made by comparing the transition dipole moments used in this work to radiative lifetimes, τ. Simard et al. (1988) report experimental lifetimes for the $B^1\Pi$ ($v' = 0$, 1, 2, and 3) states obtained from laser-induced fluorescence spectroscopy of supersonically cooled ZrO as shown in Table 6. Langhoff & Bauschlicher (1990) also calculated a $v' = 0$ lifetime of 56.4 ns as mentioned above (Table 6). The band strengths in Table 4 can be converted to Einstein A values ($A = 3.136 \times 10^{-7}\ \nu^3 S$) and to lifetimes τ, calculated as $\tau(v') = 1/\Sigma A_{v'\text{-}v''}$, summing over the v'' levels (Table 6). The average error between our lifetimes and Simard's is ±14%, with a high of ±18% for $v' = 0$. Littleton et al. (1993) reported an R_e^2 transition moment value of $2.1 \pm 0.4\ e^2A_0^2$ ($5.34 \pm 1.02\ D^2$) measured via absorption spectroscopy. This compares to our S_{0-0} LEVEL value of 9.79 D^2 with an 83% error. With these comparisons in mind, we estimate our error in the line strengths to be about 20%.

Table 6
Comparison of $^{90}Zr^{16}O$ $B^1\Pi$ ($v = 0$, 1, 2, 3, 4) Radiative Lifetimes, τ

v′	τ (ns) This Work	Experiment[a]	Theory[b]
0	68.5	83	56.4
1	69.2	83	…
2	70.8	83	…
3	81.9	90	…

Notes. Simard et al. (1988) reported their lifetimes without indicating error limits.
[a] Simard et al. (1988).
[b] Langhoff & Bauschlicher (1990).

A comparison between line positions and oscillator strengths of our line list and those of the Plez et al. (2003) line list was performed for a selected subset of bands. We found that the average difference between our PGOPHER line position and that of Plez et al. (2003) for $J'' < 100$ was 0.156 cm^{-1} and ranged from 0.026 to 0.881 cm^{-1}, depending which band was looked at. This increased to an average difference of 9.48 cm^{-1} for $J'' > 100$ with a range of 0.162–72.0 cm^{-1} depending on the band of interest. Similarly, the oscillator strengths for $J'' < 100$ were on average 14% different with a range of 0.3%–80%. This difference increased to an average of 51% for $J'' > 100$ with a range of 2.6%–370% depending on the band of interest. Over all, the two line lists agree modestly for $J'' < 100$ but deviated notably for $J'' > 100$.

4. Conclusion

A high-resolution spectrum of hot ZrO was analyzed in the near-IR and visible regions. Lines associated with the 0–0, 0–1, 0–2, 1–0, 1–2, 1–3, 2–0, 2–1, 2–3, 2–4, 3–1, 3–4, and 4–2 bands of the $B^1\Pi$—$X^1\Sigma^+$ transition were observed and fitted in PGOPHER, and updated spectroscopic constants are reported. Ab initio calculations of the transition dipole moment were used in order to determine line strengths. For the first time a line list that includes line strengths is reported. Such a line list is necessary for accurate identification and modeling of ZrO in S-type stars.

The National Solar Observatory (NSO) is operated by the Association of Universities for Research in Astronomy, Inc.

(AURA), under cooperative agreement with the National Science Foundation. Financial support was provided by the NASA Laboratory Astrophysics Program (80NSSC18K0240 and 80NSSC21K1463).

ORCID iDs

Jason J. Sorensen https://orcid.org/0000-0001-7093-7278
Peter F. Bernath https://orcid.org/0000-0002-1255-396X

References

Balfour, W. J., & Tatum, J. B. 1973, JMoSp, 48, 313
Beaton, S. A., & Gerry, M. C. L. 1999, JChPh, 110, 10715
Bernath, P. F. 2020, Spectra of Atoms and Molecules (4th ed.; Oxford: Oxford Univ. Press)
Bobrovnikoff, N. T. 1934, ApJ, 79, 483
Huang, W. J., Wang, M., Kondev, F. G., Audi, G., & Naimi, S. 2021, ChPhC, 45, 030002
Keenan, P. C. 1954, ApJ, 120, 484
Keenan, P. C., & Boeshaar, P. C. 1980, ApJS, 43, 379
King, A. S. 1924, PASP, 36, 140
Langhoff, S. R., & Bauschlicher, C. W. 1988, JChPh, 89, 2160
Langhoff, S. R., & Bauschlicher, C. W. 1990, ApJ, 349, 369
Le Roy, R. J. 2017a, JQSRT, 186, 158
Le Roy, R. J. 2017b, JQSRT, 186, 167
Littleton, J. E., & Davis, S. P. 1985, ApJ, 296, 152
Littleton, J. E., Davis, S. P., & Song, M. 1993, ApJ, 404, 412
McKemmish, L. K., Borsovszky, J., Goodhew, K. L., et al. 2018, ApJ, 867, 33
Merrill, P. W. 1922, ApJ, 56, 457
Pettersson, A., Koivisto, R., Lindgren, B., et al. 2000, JMoSp, 200, 65
Phillips, J. G., & Davis, S. P. 1976, ApJS, 32, 537
Piccirillo, J. 1980, MNRAS, 190, 441
Plez, B., Van Eck, S., & Jorissen, A. 2003, in IAU Symp. 210, Modelling of Stellar Atmospheres, ed. N. Piskunov, W. W. Weiss, & D. F. Fray (Cambridge: Cambridge Univ. Press), A2
Richardson, R. S. 1931, PASP, 43, 76
Simard, B., Mitchell, S. A., Humphries, M. R., & Hackett, P. A. 1988, JMoSp, 129, 186
Sriramachandran, P., & Shanmugavel, R. 2012, NewA, 17, 640
Suenram, R. D., Lovas, F. J., Fraser, G. T., & Matsumura, K. 1990, JChPh, 92, 4724
Tabet, J., Adem, Z., & Taher, F. 2019, Comput. Theor. Chem., 1160, 31
Van Eck, S., Neyskens, P., Jorissen, A., et al. 2017, A&A, 601, A10
Wang, M., Huang, W. J., Kondev, F. G., Audi, G., & Naimi, S. 2021, ChPhC, 45, 030003
Western, C. M. 2017, JQSRT, 186, 221
Zijlstra, A. A., Bedding, T. R., Markwick, A. J., et al. 2004, MNRAS, 352, 325